Int. J. Electrochem. Sci., 7 **(2012)** 7179 - 7205

International Journal of
ELECTROCHEMICAL
SCIENCE
www.electrochemsci.org

Theoretical Studies on Phenazine and Related Compounds as Corrosion Inhibitors for Mild Steel in Sulphuric Acid Medium

Mwadham M. Kabanda[*], *Lutendo C Murulana, Eno E. Ebenso*

Department of Chemistry, School of Mathematical & Physical Sciences, North-West University(Mafikeng Campus), Private Bag X2046, Mmabatho 2735, South Africa
[*]E-mail: mbyechura@gmail.com

Received: 1 June 2012 / *Accepted:* 3 July 2012 / *Published:* 1 August 2012

Density functional theory (DFT), using the B3LYP functional, was utilized to study the molecular properties of phenazine (PNZ), phenothiazine (PNTZ), phenoxazine (PNXZ) and 1,12-phenathroline (PNTLD) compounds in order to determine the relationship between molecular structure and corrosion inhibition efficiencies. The experimental results show that the order of inhibition efficiency is PNTLD > PNTZ > PNXZ > PNZ. The quantum chemical studies indicate that several quantum chemical parameters correlate well with the measured inhibition efficiencies of the compounds. Protonation affects the molecular properties of all the compounds studied. The results of the calculations in water solution also show that the solvent effects have significant influence on the molecular properties of the compounds. The interaction between the metal ion and each of the compounds reveal that charge transfer mechanism may be responsible for the binding of these compounds onto the metal surface. The quantitative structure activity relationship (QSAR) approach has been used and reasonable correlation of the composite index of some of the quantum chemical parameters was performed to characterize the inhibition performance of these compounds. The results showed that the %IE of the phenazine and related compounds was directly related to some of the quantum chemical parameters with varying R2 values. The experimental data obtained fits the Langmuir adsorption isotherm.

Keywords: corrosion inhibitors, DFT; adsorption mechanism, QSAR approach; molecular properties

1. INTRODUCTION

Corrosion of mild steel in acidic medium poses great economic challenges to industries that utilize mild steel produced equipments for the transportation and storage of substances that have corrosive properties. Some of the problems arising from the corrosion of equipments made from mild steel (e.g., a reaction vessel in a chemical plant) include leakage of products – what leads to loss in productivity – and contamination of reaction contents by aqueous corrosion products –leading to

undesirable results. When the effects of corrosion on equipments made from mild steel are left unattended, the industry may have to close down because of equipment failure and poor productivity. Several approaches are therefore employed to attempt to reduce the corrosion process of mild steel and one of these approaches is the use of corrosion inhibitor [1]. Corrosion inhibitors are substances that adsorb physically or chemically or both physically and chemically onto the metal-solution interface, thereby blocking the metal from coming into contact with the corrosive medium [2]. The efficient adsorption of the corrosion inhibitor onto the metal surface depends to some extent on the properties of the inhibitors, namely molecular volume (MV); molecular mass (MM); geometric parameters such as steric influences, electronic parameters such as electron density and dipole moment. The electron density of the compound depends on the functional groups present in the compounds such as heteroatoms (e.g., N, O, S and P), aromatic rings and conjugate π double bonds [3]. Compounds with high electron density interact with the metal surface by donating electrons to the vacant or partially filled d orbital of the metal, thereby resulting in a coordination bond between the metal and the inhibitor [4, 5].

Quantum chemical methods are often utilized to elucidate the physicochemical properties of compounds of interest in order to understand their interaction mechanism with the metal surface and to elucidate the centers in the compounds on which such interactions are likely to occur. In the current work, density functional theory is utilized to obtain some properties of phenazine (PNZ), phenothiazine (PNTZ), phenoxazine (PNXZ) and 1, 12-phenathroline (PNTLD) so as to investigate the relationship between their molecular structure and corrosion inhibition. The mechanism of interaction between the metal and the selected compounds is also investigated. Quantitative structure activity relationships were also developed to correlate the experimentally determined inhibition efficiency with the theoretically estimated inhibition efficiency obtained using the gravimetric method. The schematic representation of the compounds and atom numbering are shown in Fig. 1.

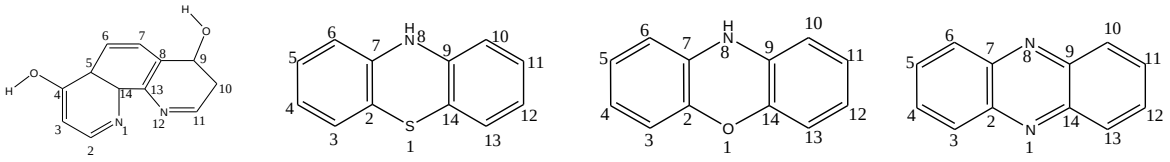

1,12-phenathroline (PNTDL) **Phenothiazine (PNTZ)** **Phenoxazine (PNXZ)** **Phenazine (PNZ)**

Figure 1. Schematic representation of the molecular structures of the studied compounds and the numbering of the atoms

2. COMPUTATIONAL DETAILS

Calculations were done using the Density Functional Theory (DFT) method with the B3LYP functional using the 6-31G (d,p) and 6-31+G (d,p) basis sets. The addition of diffuse functions is meant to investigate their influence on the calculated molecular properties. The UB3LYP/6-31+G(d,p) method was selected for the study of the radicals because of the importance of polarization and diffuse functions in describing radical anions as well as the electron delocalization effect [6]. The

DFT/B3LYP combination is known to produce good estimate of molecular properties related to molecular reactivity [7]. Among the molecular properties that are well reproduced by the DFT/B3LYP method include the energy of the highest occupied molecular orbital (HOMO), energy of the lowest unoccupied molecular orbital (LUMO), electronegativity, global hardness and softness, electron affinity, ionization potential, etc. According to Koopmans' theorem [7, 8], the electronegativity, global hardness and softness, electron affinity and ionization potential may be defined in terms of the energy of the HOMO and the LUMO. Electronegativity (χ) is the measure of the power of an electron or group of atoms to attract electrons towards itself [9], it can be estimated by using the equation:

$$\chi \cong -\tfrac{1}{2} (E_{HOMO} + E_{LUMO}) \quad (1)$$

Chemical hardness (η) measures the resistance of an atom to a charge transfer [10], it is estimated by using the equation:

$$\eta \cong -\tfrac{1}{2} (E_{HOMO} - E_{LUMO}) \quad (2)$$

Chemical softness (σ) is the measure of the capacity of an atom or group of atoms to receive electrons [10], it is estimated by using the equation:

$$\sigma = 1/\eta \cong -2/(E_{HOMO} - E_{LUMO}) \quad (3)$$

where η is the global hardness value.

Global electrophilicity index (ω) is the measure of the electrophilic tendency of a molecule; it is estimated by using the electronegativity and chemical hardness parameters through the equation:

$$\omega = \chi^2/2\eta \quad (4)$$

Electron affinity (A) is defined as the energy released when a proton is added to a system [11]. It is related to E_{LUMO} through the equation:

$$A \cong - E_{LUMO} \quad (5)$$

Ionization potential (I) is defined as the amount of energy required to remove an electron from a molecule [11]. It is related to the energy of the E_{HOMO} through the equation:

$$I \cong - E_{HOMO} \quad (6)$$

The change in the number of electrons transferred is estimated through the equation

$$\Delta N = X_{Fe} - X_{inh} / 2(\eta_{Fe} - \eta_{inh}) \quad (7)$$

where X_{Fe} and X_{inh} denote the absolute electronegativity of iron and the inhibitor molecule respectively; η_{Fe} and η_{inh} denote the absolute hardness of iron and the inhibitor molecule respectively. The values of X_{Fe} and η_{Fe} are taken as 7 $eVmol^{-1}$ and 0 $eVmol^{-1}$ respectively [12],

Frequency calculations were performed on optimized geometries to establish the nature of the stationary point on the potential energy surface. Calculations in solution were performed by utilizing the SM8 model in-cooperated in the Spartan program [13]. All optimization calculations were performed by utilizing the Spartan program. The quantitative structure activity relationship were performed using the xlstart program [14]

The inhibition efficiency of the phenazine and related compounds was obtained experimentally using the gravimetric method as reported earlier [4] in H_2SO_4 medium at different concentrations (0.01 – 0.10M) at 303 and 313K.

3. RESULTS AND DISCUSSION

3.1. Results of the calculations in vacuo and in water solution for the non-protonated species

3.1.1 Results in vacuo for the non-protonated species

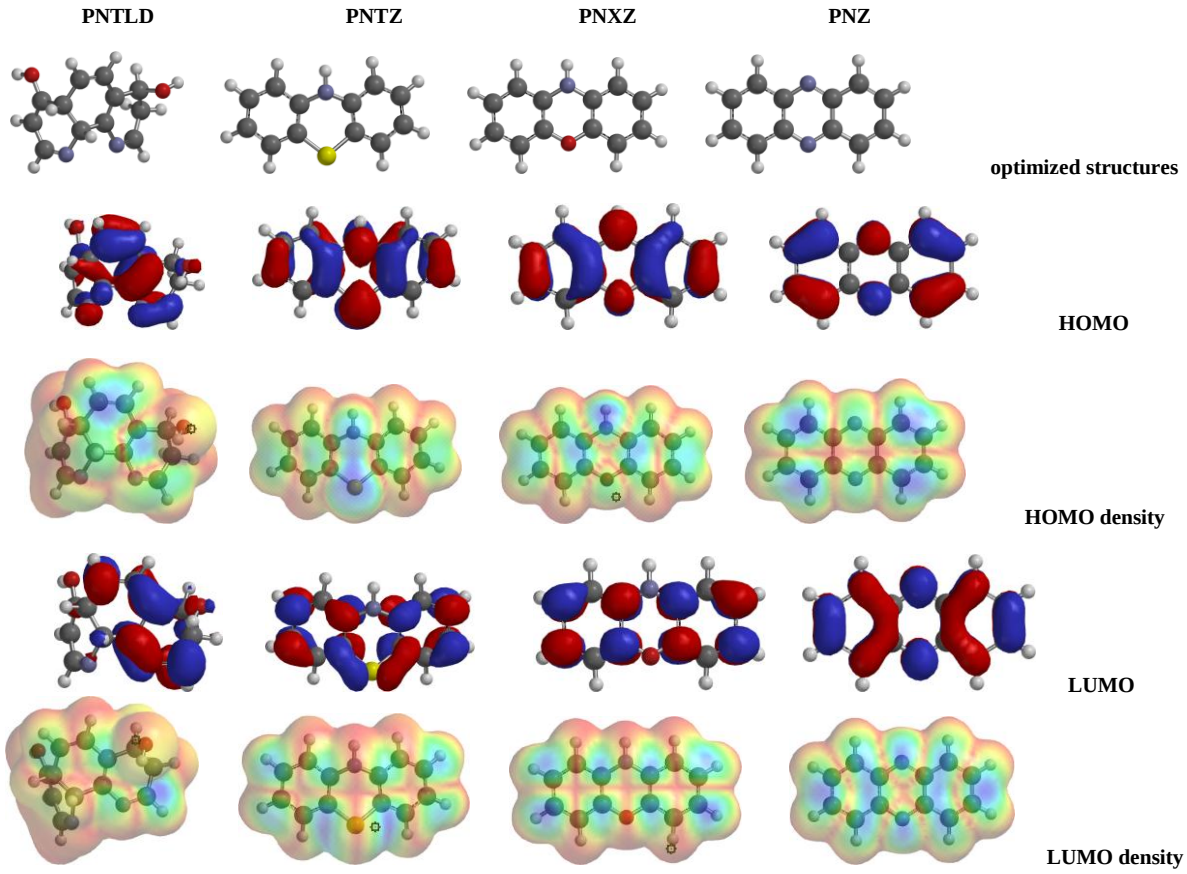

Figure 2. Optimized structures, HOMO, LUMO and the corresponding densities for the studied compounds (B3LYP/6-31G (d,p) results *in vacuo*).

Table 1. Bond length (Å) and Mulliken bond order for the studied compounds (B3LYP/6-31G(d,p) results *in vacuo*)

PNTLD			PNTZ			PNXZ			PNZ		
Bond	Bond length	Bond order	Bond	Bond length	Bond order	Bond	Bond length	Bond order	Bond	Bond length	Bond order
N1-C2	1.282	1.81	S1-C2	1.786	0.97	O1-C2	1.385	0.86	N1-C2	1.342	1.29
C2-C3	1.462	1.07	C2-C3	1.395	1.42	C2-C3	1.387	1.46	C2-C3	1.429	1.24
C3-C4	1.347	1.69	C3-C4	1.396	1.43	C3-C4	1.400	1.40	C3-C4	1.369	1.59
C4-O4	1.354	1.00	C4-C5	1.394	1.44	C4-C5	1.392	1.46	C4-C5	1.428	1.26
C4-C5	1.518	0.97	C5-C6	1.394	1.44	C5-C6	1.398	1.42	C5-C6	1.369	1.59
C5-C6	1.515	0.98	C6-C7	1.400	1.40	C6-C7	1.396	1.41	C6-C7	1.429	1.24
C6-C7	1.341	1.82	C7-N8	1.404	0.95	C7-N8	1.398	0.90	C7-N8	1.342	1.29
C7-C8	1.460	1.12	N8-C9	1.404	0.95	N8-C9	1.398	0.90	N8-C9	1.342	1.29
C8-C9	1.513	0.96	C9-C10	1.400	1.40	C9-C10	1.396	1.41	C9-C10	1.429	1.24
C9-O9	1.432	0.94	C10-C11	1.394	1.44	C10-C11	1.398	1.42	C10-C11	1.369	1.59
C9-C10	1.536	0.96	C11-N12	1.394	1.44	C11-C12	1.392	1.46	C11-N12	1.428	1.26
C10-C11	1.505	0.97	N12-C13	1.396	1.43	C12-C13	1.400	1.40	N12-C13	1.369	1.59
C11-N12	1.283	1.81	C13-C14	1.395	1.42	C13-C14	1.387	1.46	C13-C14	1.429	1.24
N12-C13	1.407	1.06	C2-C7	1.406	1.34	C2-C7	1.406	1.33	C2-C7	1.447	1.16
C13-C14	1.532	0.93	C9-C14	1.406	1.34	C9-C14	1.406	1.33	C9-C14	1.447	1.16
C13-C8	1.359	1.64	S1-C14	1.787	0.97						

Table 2. The molecular properties[a] for the investigated compounds (Results with different methods *in vacuo*. All the energies are in eV)

Structure	E_{HOMO}	E_{LUMO}	ΔE	μ	MV	Pol	IP	EA	χ	η	σ	ΔN	ω
B3LYP/6-31G(d,p)													
PNTLD	–5.594	–1.528	4.066	3.48	214	57.76	5.594	1.528	3.561	2.033	0.492	0.492	**0.846**
PNTZ	–5.007	–0.424	4.583	2.24	201	56.62	5.007	0.424	2.715	2.292	0.436	0.436	**0.935**
PNXZ	–4.791	–0.221	4.570	1.88	192	55.84	4.791	0.221	2.506	2.285	0.438	0.438	**0.983**
PNZ	–6.086	–2.428	3.657	0.01	190	55.89	6.086	2.428	4.257	1.829	0.547	0.547	**0.750**
B3LYP/6-31+G(d,p)													
PNTLD	–5.913	–1.928	3.985	3.76	214	57.80	5.913	1.928	3.921	1.993	0.502	0.773	**3.857**
PNTZ	–5.298	–0.802	4.496	2.17	202	56.66	5.298	0.802	3.050	2.248	0.445	0.879	**2.069**
PNXZ	–5.142	–0.620	4.522	1.91	192	55.86	5.142	0.620	2.881	2.261	0.442	0.911	**1.836**
PNZ	**–6.377**	**–2.764**	**3.612**	**0.00**	**190**	**55.91**	**6.377**	**2.764**	**4.571**	**1.806**	**0.554**	**0.673**	**5.783**

[a] ΔE is the energy difference between E_{HOMO} and E_{LUMO}; μ is the dipole moment in Debye; MV is the molecular volume in $Å^3$; pol is the polarization; IP is the ionization potential; EA is the electron affinity; χ is the electronegativity; η is the hardness; ΔN is the amount of electrons transferred and ω is the electrophilicity index values.

The optimized geometries of the studied compounds are shown in Fig. 2 together with the HOMO, the LUMO and their densities respectively. Table 1 show the bond length and bond order for the investigated compounds. In PNTLD, the longest bonds are the C–C single (σ) bonds and the shortest bonds are the C=C and N=C double bonds; structures PNTZ, PNTX and PNZ are all symmetric about a plane through the heteroatoms in the heterocyclic ring. In PNTZ, the longest bond is the C–S bond which suggests that this is the weakest bond and may have anti-bonding character. In structure PNTX, the weakest bonds (i.e., longest bonds) are the C–O and C–N bonds. Moreover, the fact that the O1–C2 bond is equal to the O1–C14 bond suggests that there is charge delocalization in the O1–C2–C14 region and in PNZ, the C–N bond are the shortest and the C–N–C region also shows charge delocalization.

Table 2 shows the quantum chemical parameters computed for the purpose of analyzing the reactivity of the molecules. The shape and symmetry of the HOMO and the LUMO (Fig. 2) are important in predicting the reactivity of a molecule as well as predicting the direction of chemical reactions [15]. The analysis of the HOMO indicates the regions of the molecule that have a tendency to donate electrons to electrophilic species while the analysis of the LUMO predicts the regions of the molecule with high tendency to accept electrons from nucleophilic species. The results show that the HOMO and the LUMO are delocalized throughout the molecules of the selected compounds. The HOMO and the LUMO densities, reported in Fig. 2 are meant to provide a better analysis of the regions of the molecules on which the HOMO and the LUMO has the highest localization; the blue color of the HOMO and the LUMO densities shows the regions that have the highest distribution of the HOMO and the LUMO respectively while the red color of the HOMO and the LUMO densities shows regions (in the molecules) that have minimal distribution of the HOMO and the LUMO respectively. In PNTLD, the HOMO has the highest distribution on the C6=C7 and C8=C13 double bonds, which implies that these are the regions of the molecule with the highest tendency to donate electrons; the LUMO is strongly localized on C11 atom. In PNTZ, the HOMO is spread in the region between the heteroatoms S1 and N8. The lone pair of electrons on S and N atoms are directed equatorially and tends to spread their electron density in the region between S1 and N8 atoms, which may account for the observation that this region is of high HOMO density; the LUMO is spread out almost on all the atoms of the two aromatic rings fused to the heterocyclic ring. In PNXZ, the HOMO is strongly localized on N8 and partially distributed on C4–C5, C2–C7 and C9–C14 double bonds; the LUMO is spread throughout the molecule. In PNZ, the HOMO is spread on C3, C6, C10 and C13 atoms while the LUMO is spread throughout the molecule. Therefore, PNXZ and PNZ would preferentially engage in back-donation mechanism, meaning that these compounds would donate electrons (from the HOMO) to the partially filled d orbitals of the metal and in turn the metal would donate some of its electrons to the LUMO of these compounds.

The property considered in this work for the investigated compounds is the molecular volume (MV). Molecular volume determines the surface coverage of the inhibitor on the metal surface. The compound that would have the highest surface coverage of the metal usually corresponds to that with greatest inhibition efficiency. A comparison of the MV values across structures show the order PNTLD > PNTZ > PNXZ > PNZ. Therefore the order of inhibition efficiency would preferentially be such that PNTLD > PNTZ > PNXZ > PNZ, what agrees with experimentally determined inhibition efficiency of the compounds. The properties influencing the reactivity of the compound include the energy of the HOMO (E_{HOMO}), the energy of the LUMO (E_{LUMO}), the energy difference between the HOMO and the LUMO (ΔE), global hardness (η), global softness (σ) and the dipole moment (μ), etc. These parameters are also reported in table 2. The energy of the HOMO indicates the ability of the molecule to donate electrons [16]. The molecule with the highest E_{HOMO} has electrons that have the highest energy and therefore, has the highest tendency to donate electrons. In the investigated compounds, the order of the E_{HOMO} is such that PNXZ > PNTZ > PNTLD > PNZ, therefore PNXZ would have the greatest tendency to adsorb onto the metal surface. However this trend does not agree well with the trend in the experimentally determined inhibition efficiencies.

The energy of the LUMO indicates the tendency of the molecule to accept electrons from an electron rich species. The molecule with the lowest energy of the LUMO has the highest tendency to accept electrons. The trend in the E_{LUMO} for the calculated compounds is such that PNZ < PNTLD < PNTZ < PNXZ, what implies that PNZ would preferentially accept electrons from the metal surface. The trend in the E_{LUMO}, however, does not also correlate well with the trend in the experimentally determined inhibition efficiency. The energy difference between the E_{HOMO} and the E_{LUMO}, ΔE, informs about the reactivity of the molecule towards other chemical species. The molecule with the lowest ΔE value has the highest tendency towards reactivity and would favorably interact with the metal surface. A comparison of the ΔE values of the studied compounds shows that the trend is such that PNZ < PNTLD < PNXZ < PNTZ. This trend also does not correlate well with the trend in the experimentally determined inhibition efficiencies.

Table 3. Mulliken atomic charges on the atom of the investigated compounds (B3LYP/6-31G (d,p) results *in vacuo*)

PNTLD		PNTZ		PNXZ		PNZ	
Atom	Mulliken atomic charge	Atom	Mulliken atomic charge	Atom	Mulliken atomic charge	Atom	Mulliken atomic charge
N1	–0.388	S1	0.179	O1	–0.583	N1	–0.563
C2	0.104	C2	–0.138	C2	0.312	C2	0.265
C3	–0.168	C3	–0.116	C3	–0.137	C3	–0.092
C4	0.382	C4	–0.079	C4	–0.097	C4	–0.092
O4	–0.527	C5	–0.095	C5	–0.090	C5	–0.092
C5	–0.191	C6	–0.115	C6	–0.140	C6	–0.092
C6	–0.081	C7	0.305	C7	0.319	C7	0.265
C7	–0.079	N8	–0.652	N8	–0.696	N8	–0.563
C8	0.072	C9	0.305	C9	0.319	C9	0.265
C9	0.108	C10	–0.115	C10	–0.139	C10	–0.092
O9	–0.538	C11	–0.095	C11	–0.090	C11	–0.092
C10	–0.242	N12	–0.079	N12	–0.097	N12	–0.092
C11	–0.097	C13	–0.116	C13	–0.137	C13	–0.092
N12	–0.405	C14	–0.138	C14	0.312	C14	0.265
C13	–0.180						
C14	–0.011						

The global hardness and softness parameters are often discussed in terms of hard-soft-acid-base (HSAB) theory. According to this theory, soft acids interact preferentially with soft bases and hard acids interact preferentially with hard bases. Metals are generally considered to be soft acid [17], therefore they would preferentially interact with inhibitors that have high σ values and low η values. The σ values for the investigated compounds follow the trend PNZ < PNTLD < PNXZ < PNTZ, which is not in good agreement with experimentally determined inhibition efficiency of the inhibitors. The dipole moment informs about the polarity of the molecule. Several researchers in the area of corrosion science have established that an increase in the inhibition efficiency is related to the increase in the dipole moment [16]. The order of the dipole moment for the investigate compounds is such that PNTLD > PNTZ > PNXZ > PNZ. This trend correlates well with experimentally determined inhibition efficiency.

Table 4. The condensed Fukui functions on the atom of the studied compounds. B3LYP/6-31G (d,p) results *in vacuo*

PNTLD		PNTZ		PNXZ		PNZ	
Atom	f^- function	Atom	f^- function	Atom	f^- function	Atom	f^- function
N1	–0.042	S1	–0.223	O1	–0.067	N1	–0.056
C2	–0.017	C2	0.004	C2	0.649	C2	–0.011
C3	–0.017	C3	–0.012	C3	–0.020	C3	–0.044
C4	–0.009	C4	–0.030	C4	–0.030	C4	–0.025
O4	–0.023	C5	–0.015	C5	–0.017	C5	–0.025
C5	0.031	C6	–0.023	C6	–0.027	C6	–0.044
C6	–0.055	C7	0.618	C7	–0.011	C7	–0.011
C7	–0.025	N8	–0.062	N8	–0.077	N8	–0.056
C8	–0.036	C9	0.618	C9	–0.011	C9	–0.011
C9	0.009	C10	–0.023	C10	–0.026	C10	–0.044
O9	–0.045	C11	–0.015	C11	–0.017	C11	–0.025
C10	0.027	N12	–0.030	N12	–0.030	N12	–0.025
C11	–0.243	C13	–0.012	C13	–0.020	C13	–0.044
N12	–0.030	C14	0.005	C14	0.649	C14	–0.011
C13	–0.414						
C14	0.028						
	f^+ function		f^+ function		f^+ function		f^+ function
N1	–0.002	S1	–0.174	O1	–0.013	N1	–0.078
C2	–0.204	C2	–0.014	C2	–0.043	C2	–0.015
C3	–0.003	C3	–0.002	C3	–0.004	C3	–0.031
C4	0.001	C4	–0.027	C4	–0.042	C4	–0.015
O4	–0.005	C5	–0.037	C5	–0.029	C5	–0.015
C5	0.032	C6	–0.001	C6	0.026	C6	–0.031
C6	–0.064	C7	–0.034	C7	–0.586	C7	–0.016
C7	–0.011	N8	0.001	N8	0.009	N8	–0.078
C8	–0.042	C9	–0.034	C9	–0.586	C9	–0.016
C9	0.012	C10	–0.002	C10	0.025	C10	–0.031
O9	–0.032	C11	–0.037	C11	–0.029	C11	–0.015
C10	0.045	N12	–0.027	N12	–0.041	N12	–0.015
C11	0.088	C13	–0.002	C13	–0.004	C13	–0.031
N12	–0.051	C14	–0.013	C14	–0.043	C14	–0.016
C13	0.048						
C14	0.011						

Some molecular properties do not only indicate reactivity of molecules but also indicate the site selectivity in an individual chemical species, i.e., the regions of the molecules on which certain type of reactions are likely to occur. The partial atomic charge on the atoms of the molecule is one of such parameters. The interaction between the metal and the inhibitor is often considered to preferentially take place on the atom with the highest negative charge [18]. The Mulliken atomic charges for the studied compounds are reported in table 3 and the highest negative charge on all the molecules is located on the heteroatoms, which suggests that these centers have highest electron density and would preferentially interact with the metal surface.

The other quantum chemical descriptor often utilized to investigate molecular selectivity is the condensed Fukui functions. These functions inform about the centers in a molecule on which nucleophilic, electrophilic and radical reactions are most likely to occur. The Fukui functions for the atoms in the molecule susceptible to electrophilic attack and for the atoms in the molecule susceptible to nucleophilic attack are often estimated using the finite difference approximation approach [19]

$f^+ = q_{(N+1)} - q_N$ for nucleophilic attack (8)

$f^- = q_N - q_{(N-1)}$ for electrophilic attack (9)

where $q_{(N+1)}$, q and $q_{(N-1)}$ are the charges of the atoms on the systems with N+1, N and N–1 electrons respectively. The site with the highest f^+ correspond to a possible site for nucleophilic attack while the site with the highest value of f^- correspond to a possible site for an electrophilic attack. The calculated condensed Fukui functions for the non-hydrogen atoms in the studied compounds are reported in table 4. The preferred site for nucleophilic attack is C2, C6 and C11 atoms in PNTLD; S1 atom in PNTZ; C7 and C9 in PNXZ; N1 and N8 in PNZ. The preferred site for electrophilic attack is N1, C6 and C13 in structure PNTLD; S1, C7 and C9 in PNTZ; C2 and C14 in PNXZ; N1, C3, N6, C10 and C13 in PNZ. These results agree well with the analysis of the HOMO and the LUMO as well as the analysis of the partial charge on the atoms.

3.1.2. Results in water solution for the non-protonated species

Electrochemical reactions take place in solution and therefore it is important to take into account the solvent effects when studying the interaction between metal and the inhibitors. The most interesting parameters of the solvent to consider is the solvent effect and its components i.e., the electrostatic and the non-electrostatic components. The solvent effects indicate the extent of stabilization of the solute by the solvent. The molecule that is least stabilized by the solvent (i.e., has less interaction with the water molecules) has greater tendency to interact with the metal surface while the solvent that interact with the water molecules more strongly (i.e., has the highest ΔG_{solv}) has less tendency to interact with the metal surface [20]. The components of the solvent effect indicate the preferred type of interaction between the solvent and the solute (i.e., the inhibitor molecules) and the component with the largest contribution suggests the predominant interactions between the solvent and the solute. Electrostatic interactions include the dipole-dipole, the dipole-charge and charge-charge interactions while non-electrostatic interactions include the van der Waal interactions and dispersion interactions. The solvent effects together with its components are presented in table 5.

Table 5. The Solvent effects and its components for the studied compounds (B3LYP/6-31+G (d,p) results water solution)

Structures	Solvent effect			Electrostatic component			Non-electrostatic component		
	neutral	Protonated	deprotonated	neutral	Protonated	deprotonated	neutral	protonated	deprotonated
PNTLD	–14.4789	–56.9356	–[a]	–8.5225	–52.8780	–[a]	–5.9564	–4.0576	
PNTZ	–3.0475	–46.8884	–8.0620	–1.1938	–46.1887	–5.9310	–1.8537	–0.6996	–2.1310
PNXZ	–3.3640	–53.1986	–7.7631	–1.4497	–51.4153	–5.5990	–1.9142	–1.7833	–2.1641
PNZ	–5.9333	–50.8112		–3.3511	–48.7477		–2.5822	–2.0635	

[a] on optimization the deprotonated form of PNTLD does not converge.

The order of the solvent effect in the studied compounds is PNTLD > PNZ > PNTX > PNTZ. The trend PNZ > PNTX > PNTZ agrees well with the experimentally determined inhibition efficiency (i.e., the smaller ΔG_{solv} is, the greater is the adsorbabilty of the inhibitors onto the metal surface).

However, the indication that PNTLD has the highest ΔG_{solv} and would therefore have the least tendency to interact with the metal surface does not agree with the reported experimental inhibition efficiency. It is however understandable that PNTLD would have the highest ΔG_{solv} value mainly because it has the highest number of polar bonds (due to the presence of two OH groups), and therefore it would have greater electrostatic (e.g., dipole-dipole) interactions with the water molecules. However, these polar groups may also be centers for adsorption on the metal surface and this explains the preference of PNTLD as metal corrosion inhibitor. A comparison of the components of ΔG_{solv} suggests that electrostatic interactions have strong contribution to the interaction between the water molecules and the inhibitor molecules.

The various properties of the studied compounds in water solution are reported in table 6.

Table 6. The molecular properties of the investigated compounds in water solution. (B3LYP/6-31G (d,p) results).

Quantum descriptor[a]	*In vacuo*[b]				In solution			
	PNTLD	**PNTZ**	**PNXZ**	**PNZ**	**PNTLD**	**PNTZ**	**PNXZ**	**PNZ**
E_{HOMO} (eV)	–5.594	–5.007	–4.791	–6.086	–5.611	–7.229	–4.861	–6.145
E_{LUMO} (eV)	–1.528	–0.424	–0.221	–2.428	–1.509	3.346	–0.238	–2.536
ΔE (eV)	4.066	4.583	4.570	3.657	4.102	10.575	4.623	3.609
μ (Debye)	3.48	2.24	1.88	0.01	4.85	2.45	2.48	0.00
MV, (A^3)	214	201	192	190	214	201	192	190
Pol	57.76	56.62	55.84	55.89	57.75	55.22	55.83	55.90
IP, (eV)	5.594	5.007	4.791	6.086	5.611	7.229	4.861	6.145
EA, (eV)	1.528	0.424	0.221	2.428	1.509	–3.346	0.238	2.536
χ	3.561	2.715	2.506	4.257	3.560	1.942	2.550	4.341
η	2.033	2.292	2.285	1.829	2.051	5.287	2.311	1.804
σ	0.492	0.436	0.438	0.547	0.488	0.189	0.433	0.554
ΔN	0.846	0.935	0.983	0.750	0.839	0.478	0.963	0.737
ω	3.118	1.609	1.374	4.955	3.089	0.357	1.406	5.221

[a] ΔE is the energy difference between E_{HOMO} and E_{LUMO}; μ is the dipole moment in Debye; MV is the molecular volume in $Å^3$; pol is the polarization; IP is the ionization potential; EA is the electron affinity; χ is the electronegativity; η is the hardness; σ is the global softness; ΔN is the amount of electrons transferred and ω is the electrophilicity index.
[b] The results *in vacuo* are included for comparison purposes.

The trend in the E_{HOMO} is such that PNXZ > PNTLD > PNZ > PNTZ and the trend in the E_{LUMO} is such that PNTZ > PNZ > PNTLD > PNXZ. These trends are different from those *in vacuo* showing that, unlike *in vacuo*, PNTLD is a better electron donor than PNTZ. The difference in the trend between the results i*n vacuo* and the results in water solution may be related to the solvent effects on the compounds. The trends in the E_{HOMO} and in the E_{LUMO} values also do not agree well with the trend in the experimentally determined inhibition efficiencies of the inhibitors.

A comparison of the molecular properties of the inhibitors between the results *in vacuo* and the results in water solution provides an indication of the effect of the solvent on molecular properties. E_{HOMO} is lower in water solution than *in vacuo* (0.070–2.222 eV) which indicates that the solvent effect decreases the tendency of the inhibitors to donate electrons; E_{LUMO} is lower in water solution than *in vacuo* for PNTLD and PNTZ while it is higher *in vacuo* than in water solution for PNXZ and PNZ. With the exception of PNZ , the dipole moment is always higher in water solution than *in vacuo*, and indication of the polarization effect of the solvent on the inhibitors molecules; ΔN is smaller in

water solution than *in vacuo*, which may be related to the decreased tendency of the molecule to donate electrons in water solution.

3.2. Results in vacuo and in water solution for the protonated species

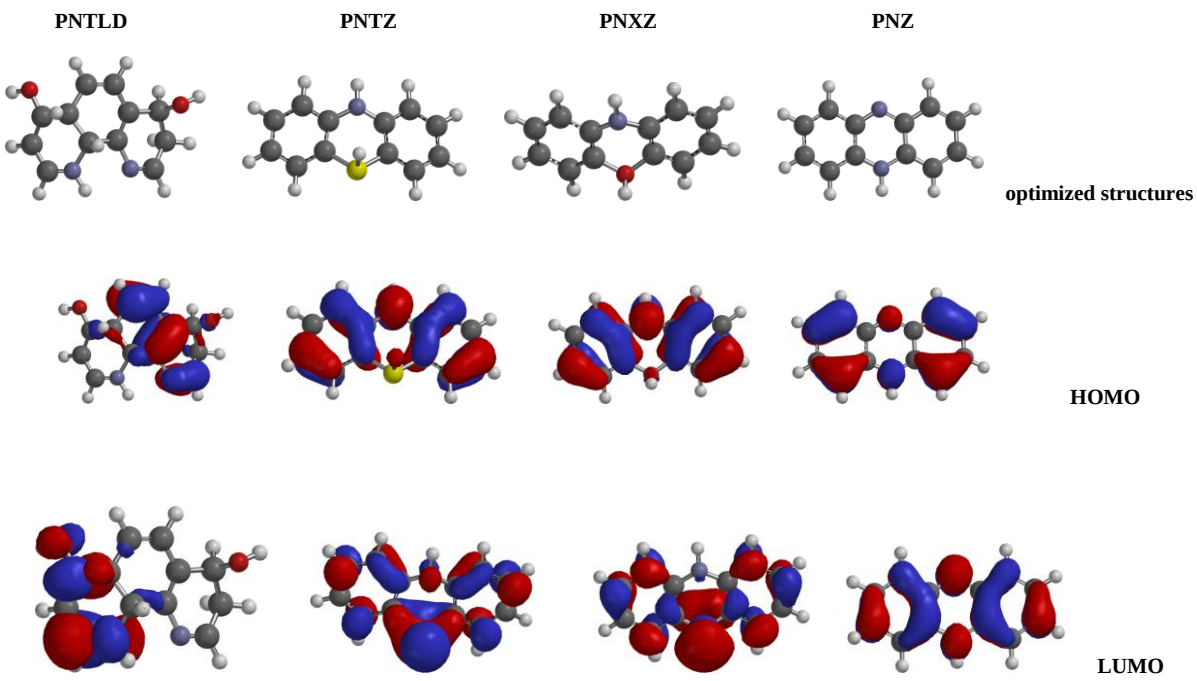

Figure 3. Optimized structures, HOMO and LUMO of the protonated species for the studied compounds (B3LYP/6-31G (d,p) results *in vacuo*).

A consideration of the protonated species of the inhibitors in acidic medium is important because acid media have a high tendency to protonated molecules that have heteroatoms. Therefore, both the neutral and protonated species would be present in solution and both species may interact with the metal surface. A study of both species provides information on the preferred species to interact with the metal surface.

The *in vacuo* optimized geometries and the corresponding HOMO and LUMO of the protonated species are shown in Fig. 3.

A comparison of Figs. 2 and 3 provides information on the variation in the distribution of the HOMO and the LUMO between the neutral and the protonated species. For instance, the LUMO density for the protonated species of PNTZ and PNXZ is strongly localized in the C2S1C14 and C2O1C14 regions respectively, a remarkable trend from the neutral species.

The variation in the geometric parameters between the protonated and the neutral species are reported in table 7. Such a comparison shows the effect of protonation on the geometry. The changes in the bond lengths are less than 0.01Å (with the exception of the N1–C2, C2–C3 and C3–C4 bonds in PNTLD) which suggests that protonation has minimal influence on the bond lengths of the inhibitors.

The bond angles varies (in both directions) by less than 3° with the exception of the ∠CNC bond angle in PNTLD and PNZ structures.

Table 7. Variations[a] in the bond lengths (Å) and bond angles (°) between the protonated and the neutral species (B3LYP/6-31G (d,p) results *in vacuo*)

PNTLD	Variation	PNTZ	Variation	PNXZ	Variation	PNZ	Variation
			bond length				
N1-C2	–0.028	S1-C2	0.007	O1-C2	–0.093	N1-C2	–0.018
C2-C3	0.053	C2-C3	–0.005	C2-C3	0.006	C2-C3	0.021
C3-C4	–0.026	C3-C4	0.007	C3-C4	0.005	C3-C4	–0.009
C4-C5	0.000	C4-C5	–0.007	C4-C5	–0.008	C4-C5	0.003
C5-C6	–0.006	C5-C6	0.004	C5-C6	0.005	C5-C6	–0.001
C6-C7	0.000	C6-C7	–0.004	C6-C7	–0.007	C6-C7	0.002
C7-C8	–0.002	C7-N8	0.011	C7-N8	0.006	C7-N8	0.003
C8-C9	–0.003						
C9-C10	–0.006						
C10-C11	0.004						
C11-N12	–0.004						
N12-C13	0.003						
C13-C14	0.008						
			Bond angle				
N1C2C3	3.1	S1C2C3	0.9	O1C2C3	0.1	C1C2C3	–3.0
C2C3C4	–0.5	C2C3C4	1.7	C2C3C4	2.9	C2C3C4	1.7
C3C4C5	–2.0	C3C4C5	0.1	C3C4C5	0.1	C3C4C5	–1.0
C4C5C6	0.2	C4C5C6	–1.2	C4C5C6	–1.4	C4C5C6	0.3
C5C6C7	–1.2	C5C6C7	0.3	C5C6C7	0.4	C5C6C7	0.3
C6C7C8	–0.9	C6C7N8	–0.6	C6C7N8	–1.2	C6C7N8	–0.2
C7C8C9	–0.5	C7N8C9	–1.5	C7N8C9	–0.9	C7N8C9	–2.7
C8C9C10	–0.9	C14S1C2	–2.2	C14O1C2	2.0	C14N1C2	–6.6
C9C10C11	–2.5						
C10C11N12	–0.3						
C11N12C13	0.5						
N12C13C14	2.9						
C14N1C2	–7.2						

[a] The differences are taken as 'value in the protonated species minus value in the neutral species'

The extent of protonation (i.e., how likely the molecule would prefer to be protonated) is estimated using the proton affinity (PA) of the inhibitors. The proton affinity is obtained using the equation

$$PA = E_{prot} + E_{H2O} - E_{non\text{-}prot} + - E_{H3O+} \quad (10)$$

where E_{prot} and $E_{non\text{-}prot}$ are the total energies of the protonated and the neutral (non-protonated) inhibitors respectively, E_{H2O} is the total energy of a water molecule and E_{H3O+} is the total energy of the hydronium ion. The results show that the PA values, for the different protonated inhibitors, are 5.81/PNTLD, 1.51/PNTZ, 0.86/PNTX and 2.61/PNZ. These results suggest that protonation on the N atom (in PNTLD and PNZ) is preferred than on S and O atoms.

Table 8. Physicochemical properties of the protonated species (B3LYP/6-31G (d,p) results *in vacuo*).

Quantum descriptor[a]	Neutral species [b]				Protonated species			
	PNTLD	**PNTZ**	**PNXZ**	**PNZ**	**PNTLD**	**PNTZ**	**PNXZ**	**PNZ**
E_{HOMO} (eV)	–5.594	–5.007	–4.791	–6.086	–9.383	–9.663	–9.648	–10.580
E_{LUMO} (eV)	–1.528	–0.424	–0.221	–2.428	–6.305	–5.022	–4.629	–7.353
ΔE (eV)	4.066	4.583	4.570	3.657	3.078	4.640	5.019	3.225
μ (Debye)	3.48	2.24	1.88	0.01	7.43	1.93	2.00	2.95
MV, (A^3)	214	201	192	190	216	204	194	192
Pol	57.76	56.62	55.84	55.89	58.18	56.80	55.98	56.19
IP, (eV)	5.594	5.007	4.791	6.086	9.383	9.663	9.648	10.58
EA, (eV)	1.528	0.424	0.221	2.428	6.305	5.022	4.629	7.353
χ	3.561	2.715	2.506	4.257	7.844	7.342	7.139	8.965
η	2.033	2.292	2.285	1.829	1.539	2.320	2.510	1.612
σ	0.492	0.436	0.438	0.547	0.650	0.431	0.398	0.620
ΔN	0.846	0.935	0.983	0.750	–0.274	–0.074	–0.028	–0.609
ω	3.118	1.609	1.374	4.955	19.990	11.617	10.153	24.925

[a] ΔE is the energy difference between E_{HOMO} and E_{LUMO}; μ is the dipole moment in Debye; MV is the molecular volume in $Å^3$; pol is the polarization; IP is the ionization potential; EA is the electron affinity; χ is the electronegativity; η is the hardness; σ is the global softness; ΔN is the amount of electrons transferred and ω is the electrophilicity index.

[b] The physicochemical properties of the neutral species *in vacuo* are included for comparison purpose

A comparison of the molecular properties of the inhibitors for the protonated and the neutral species provides information on the effects of protonation on the molecular properties. The molecular properties of the protonated species are reported in table 8; E_{HOMO} is lower (by 3.789–4.857 eV) in the protonated than in the neutral species, which indicates that protonation decreases the tendency of the inhibitors to donate electrons; E_{LUMO} is lower (by 4.408–4.925 eV) in the protonated than in the neutral species, which indicates that protonation increases the tendency of the inhibitors to accept electrons; the dipole moment is affected differently for different compounds; ΔN values indicates that the number of electron transferred by the protonated species is less than the number of electrons transferred by the non-protonated species.

The Mulliken partial atomic charges on the atoms of the protonated species are reported in table 9 and indicate that protonation on N atom results in increased negative charge on the N atom (by -0.058 for N1 in PNTLD; by -0.002 in PNXZ; by -0.099 for N1 in PNZ) and protonation on the S and O atom results in decreased charge of the atoms. This result suggests that molecules with N atoms are preferentially protonated in acidic medium while molecules with S and O atoms do not prefer to undergo protonation, which confirms the results obtained from the calculation of the proton affinity.

Table 9. Mulliken atomic charges on the atom of the protonated species (B3LYP/6-31G (d,p) results *in vacuo*).

PNTLD		PNTZ		PNXZ		PNZ	
Atom	Mulliken atomic charge	Atom	Mulliken atomic charge	Atom	Mulliken atomic charge	Atom	Mulliken atomic charge
N1	–0.487	S1	0.265	O1	–0.602	N1	–0.592
C2	0.071	C2	–0.251	C2	0.265	C2	0.235
C3	–0.171	C3	–0.121	C3	–0.137	C3	–0.103
C4	0.468	C4	–0.165	C4	–0.098	C4	–0.066
O4	–0.541	C5	–0.135	C5	–0.100	C5	–0.066
C5	–0.203	C6	–0.181	C6	–0.131	C6	–0.103
C6	–0.062	C7	0.341	C7	0.344	C7	0.234
C7	–0.077	N8	–0.786	N8	–0.717	N8	–0.592
C8	0.104	C9	0.341	C9	0.344	C9	0.235
C9	0.103	C10	–0.181	C10	–0.131	C10	–0.103
O9	–0.559	C11	–0.135	C11	–0.100	C11	–0.066
C10	–0.224	N12	–0.165	N12	–0.098	N12	–0.066
C11	0.098	C13	–0.121	C13	–0.137	C13	–0.103
N12	–0.491	C14	–0.251	C14	0.265	C14	0.234
C13	0.128						
C14	–0.019						

A comparison of the molecular properties of the protonated species *in vacuo* and in water solution provides information on the effects of the solvent on the protonated species.

Table 10. Comparison of the molecular properties of the protonated species *in vacuo* and in water solution. B3LYP/6-31G (d,p) results

a) The calculated molecular properties *in vacuo* and in water solution

Quantum descriptor#	***In vacuo***				**In water solution**			
	PNTLD	**PNTZ**	**PNXZ**	**PNZ**	**PNTLD**	**PNTZ**	**PNXZ**	**PNZ**
E_{HOMO} (eV)	–9.383	–9.663	–9.648	–10.58	–5.819	–5.910	–5.700	–6.685
E_{LUMO} (eV)	–6.305	–5.022	–4.629	–7.353	–2.021	–1.180	–0.610	–3.437
ΔE (eV)	3.078	4.640	5.019	3.225	3.798	4.721	5.090	3.248
μ (Debye)	7.43	1.93	2.00	2.95	9.58	2.90	2.70	4.55
MV, (A^3)	216	204	194	192	216	203	194	192
Pol	58.18	56.80	55.98	56.19	58.00	56.76	55.94	56.17
IP, (eV)	9.383	9.663	9.648	10.58	5.819	5.910	5.700	6.685
EA, (eV)	6.305	5.022	4.629	7.353	2.021	1.180	0.610	3.437
χ	7.844	7.342	7.139	8.965	3.920	3.545	3.160	5.061
η	1.539	2.320	2.510	1.612	1.899	2.361	2.545	1.624
σ	0.650	0.431	0.398	0.620	0.527	0.424	0.393	0.616
ΔN	–0.274	–0.074	–0.028	–0.609	0.811	0.732	0.754	0.597
ω	19.990	11.617	10.153	24.925	4.046	2.661	1.962	7.886

#ΔE is the energy difference between E_{HOMO} and E_{LUMO}; μ is the dipole moment in Debye; MV is the molecular volume in $Å^3$; pol is the polarization; IP is the ionization potential; EA is the electron affinity; χ is the electronegativity; η is the hardness; σ is the global softness; ΔN is the amount of electrons transferred and ω is the electrophilicity index

b) Variation in molecular properties of the protonated species between the results *in vacuo* and the results in water solution.

Quantum descriptor	Variation in the molecular properties*			
	PNTLD	**PNTZ**	**PNXZ**	**PNZ**
ΔE_{HOMO} (eV)	3.564	3.753	3.948	3.895
ΔE_{LUMO} (eV)	4.284	3.842	4.019	3.916
$\Delta(\Delta E)$ (eV)	0.720	0.081	0.071	0.023
$\Delta\mu$ (Debye)	2.15	0.97	0.70	1.60
ΔPol	–0.18	–0.04	–0.04	–0.02
ΔIP, (eV)	–3.564	–3.753	–3.948	–3.895
ΔEA, (eV)	–4.284	–3.842	–4.019	–3.916
$\Delta\chi$	–3.924	–3.797	–3.979	–3.904
$\Delta\eta$	0.360	0.041	0.035	0.012
$\Delta\sigma$	–0.123	–0.007	–0.005	–0.004
Δ (ΔN)	1.085	0.806	0.782	1.206
$\Delta\omega$	–15.944	–8.956	–8.191	–17.039

*The differences (Δ values) are taken as 'value of a given molecular property in water solution minus the corresponding value of that particular molecular property *in vacuo*'.

Table 10 shows the molecular properties of the protonated species in water solution and compares with the corresponding molecular properties *in vacuo* solution. Both the HOMO and the LUMO energies are higher in water solution than *in vacuo*, which indicates that in water solution the ability of the protonated inhibitors to donate electrons is higher while its ability to accept electrons is lower; ΔE values indicates that the reactivity of the protonated species in water solution is decreased as compared to the reactivity *in vacuo*;

The dipole moment is slightly higher in water solution than *in vacuo* as a result of increased polarization of the solute by the solvent molecules.

3.3. Results in vacuo and in water solution for the deprotonated species

Radical reactions are known to occur in electrochemical systems because of the presence of reactive oxygen species in electrochemical solution. This means that neutral species, protonated species and deprotonated (i.e., radical) species of the inhibitors co-exist in electrochemical systems and all are capable of adsorbing physically and/or chemically onto the metal surface, for instance, the deprotonated species of the triazole and its derivatives as potential corrosion inhibitors have been studied extensively [21, 22]. Inhibitors with OH or NH groups are capable of scavenging the free radical species (i.e., the reactive O or N species) according to H atom transfer (HAT) mechanism or the electron transfer (ET) mechanism [6].

H atom transfer mechanism: $R'OH + R^{\bullet} \rightarrow R'O^{\bullet} + RH$ (11)

Electron transfer mechanism: $R'OH + R^{\bullet} \rightarrow R'OH^{+} + R^{-} \rightarrow R'O^{\bullet} + RH$ (12)

The discussion in the next sections considers the possibility of the HAT mechanism for the formation of the deprotonated inhibitor and attempts to identify the possible sites in the molecule on

which the deprotonated species may interact with the metal surface. Only PNTLD, PNTZ and PNXZ inhibitors are considered because of the presence of the OH and NH groups in these compounds; in PNTLD, the loss of the $H^{\bullet}$ atom from the OH group results in the $R'O^{\bullet}$ deprotonated species while in both, PNTZ and the PNXZ compound the loss of the $H^{\bullet}$ results in the formation of the $R'N^{\bullet}$ deprotonated species. The most significant quantum chemical property to take into consideration when studying deprotonated species is the total spin density. This parameter informs about the distribution of the electron spin which in turn determines the stability of the deprotonated species. The more stable radicals are the most preferred and they are often characterized by spin delocalization of the unpaired electrons. In the next sections the results *in vacuo* and in water solutions for the deprotonated species are presented and analyzed in terms of the spin density of the species.

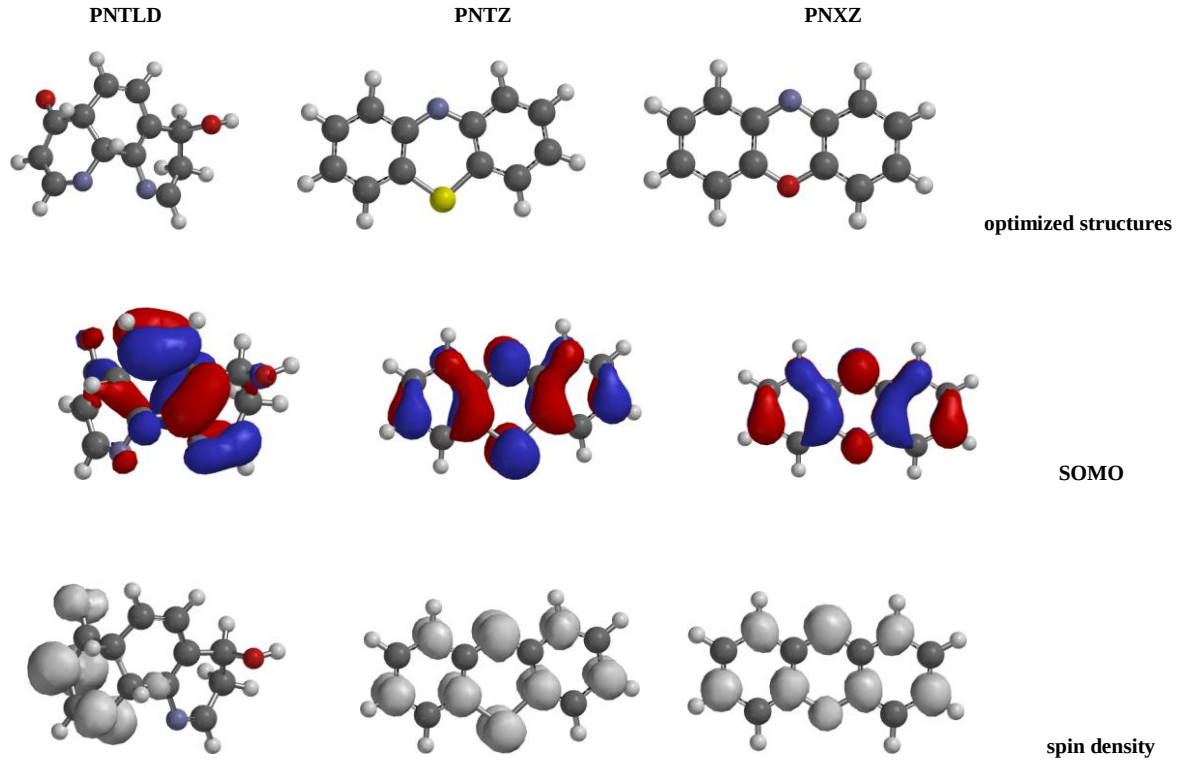

Figure 4. Optimized structures, Singly Occupied Molecular orbital (SOMO) and the spin density distribution for the lowest-energy deprotonated species (B3LYP/6-31G (d,p) results *in vacuo*).

The optimized geometries of the deprotonated species of PNTLD, PNTZ and PNXZ are shown in Fig. 4 together with their corresponding SOMO (Singly Occupied Molecular Orbital) and spatial spin densities formed after the HAT mechanism. A map of spin density reveals the location of unpaired electron and informs about the extent to which the radical site remains localized or is delocalized within a given radical species. In PNTLD radical, the spin density is delocalized strongly on N1, C3 and O4 atoms with the spin density values (au) of 0.479, 0.690 and 0.182 respectively; in PNTZ radical, the spin density is delocalized on alternating C atoms of the aromatic rings and on S1

and N8 atoms of the heterocyclic ring; in PNXZ, the spin density is also delocalized on alternating carbon atoms of the aromatic rings and on the O1 and N8 atoms of the heterocyclic ring. Since spin density delocalization is highest in PNTZ and PNTX, these structures form more stable radicals than PNTLD.

Table 11. The molecular properties for the deprotonated species calculated at B3LYP/6-31+G (d,p) *in vacuo*

Quantum descriptor [a]	Neutral species			Deprotonated species		
	PNTLD	**PNTZ**	**PNXZ**	**PNTLD**	**PNTZ**	**PNXZ**
E_{HOMO} (eV)	–5.913	–5.298	–5.142	–6.177	–4.979	–5.062
E_{LUMO} (eV)	–1.928	–0.802	–0.620	–2.189	–1.117	–0.972
ΔE (eV)	3.985	4.496	4.522	3.988	3.862	4.090
μ (Debye)	3.76	2.17	1.91	1.18	1.20	1.34
MV, (A^3)	214	202	192	212	199	189
IP, (eV)	57.80	56.66	55.86	6.177	4.979	5.062
EA, (eV)	5.913	5.298	5.142	2.189	1.117	0.972
χ	3.921	3.050	0.620	4.183	3.048	3.017
η	1.993	2.248	2.881	1.994	1.931	2.045
σ	0.502	0.445	2.261	0.501	0.518	0.489
ΔN	0.773	0.879	0.442	0.706	1.023	0.974
ω	3.857	2.069	0.911	4.387	2.406	2.226

[a] ΔE is the energy difference between E_{HOMO} and E_{LUMO}; μ is the dipole moment in Debye; MV is the molecular volume in $Å^3$; pol is the polarization; IP is the ionization potential; EA is the electron affinity; χ is the electronegativity; η is the hardness; σ is the global softness; ΔN is the amount of electrons transferred and ω is the electrophilicity index

Table 11 reports the molecular properties of the radical species; the energy of the SOMO informs about the tendency of a deprotonated species to electron donation. A comparison of the HOMO of the neutral species and the SOMO of the deprotonated species suggests that the deprotonated species would have greater tendency to donate its electron to the vacant s or d orbitals of the metal. Moreover, ΔE suggests that the deprotonated species are more reactive than the corresponding neutral species. The dipole moment of the deprotonated species is smaller than the corresponding dipole moment for the neutral species.

3.4. Interaction mechanism between the metal ion and the inhibitor molecules in vacuo

The modeling of the interaction between the inhibitor and the metal surface assumes that the metal ion chelation ability with the inhibitor is related to the corrosion inhibition efficiency [23-28]. As discussed earlier, electrochemical reactions take place in solution, where iron would preferentially be in an ionic form (i.e., in the Fe^{2+} or Fe^{3+} ionic). Initially the isolated Fe^{2+} ion was optimized at the same level of theory as the inhibitor and its energy and electron distribution determined; then the optimized Fe^{2+} ion was made to interact with the inhibitor by placing it in the vicinity of the electron donor centers of the inhibitor and optimizing the resulting geometry. The optimized complexes were analyzed to determine the regions of the molecule that donated electrons to the metal ion; the orbital in the iron metal that received the electrons; the amount of charge transferred and the strength of interaction between the metal and the inhibitor (i.e., the metal ion affinity). The change in the Mulliken

bond order of the bonds between the isolated inhibitor and the complexed inhibitor indicates the variations in the electron density in the given bonds. A smaller value of bond order for the complexed inhibitor indicates that there is a decrease in the charge density/electron density in the given bond.

The strength of the interaction between the metal and the inhibitors may be evaluated using the equation;

$$E_{inter} = E_{complex} - \sum (E_{Fe}^{2+} + E_{inhibitor}) \quad (13)$$

where $E_{complex}$ is the total energy of the optimized complex, E_{Fe}^{2+} is the total energy of the isolated $_{Fe}^{2+}$ ion and $E_{inhibitor}$ is the total energy of the isolated inhibitors. The distance between the donor atoms and the Fe atom also indicates the strength of the interactions between the metal and the inhibitor; a shorter distance indicates strong interactions while a longer distance indicates weaker interactions.

For each inhibitors, Fe^{2+} ion was placed in the vicinity of the electron rich centers and optimized; in structure PNTLD, the Fe^{2+} ion was placed separately in the vicinity of N1 and N12; in structure PNTZ, the Fe^{2+} ion was place in the vicinity of S1 and in the vicinity of N8 atoms and optimized separately; in structure PNXZ, the Fe^{2+} ion was place in the vicinity of O1 and in the vicinity of N8 atoms and optimized separately; in structure PNZ, the Fe^{2+} ion was place in the vicinity of N1 atom and optimized.

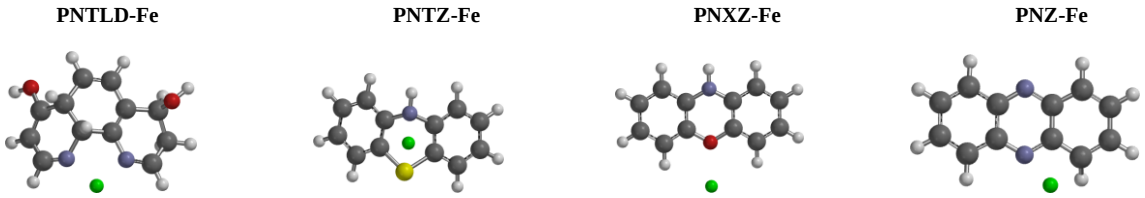

Figure 5. Optimized inhibitor-metal complexes for the studied compounds (B3LYP/6-31G (d,p) results *in vacuo*).

Table 12. Interaction energy (ΔE_{inter}, kcal/mol) between the metal and the inhibitor and the bond distance (Å) between the metal and the inhibitor atoms. B3LYP/6-31G (d,p) results *in vacuo*

Complex	ΔE_{inter} kcal/mol	Fe···inhibitor separation in Å					
		Fe···N1	Fe···S1	Fe···O1	Fe···N8	Fe···N12	Fe···C13
PNTLD-Fe	–262.009	1.923				1.989	
PNTZ-Fe	–202.254		2.347		2.031		
PNXZ-Fe	–180.071			2.318			
PNZ-Fe	–186.505	1.977					2.169

The geometries of the optimized complexes are shown in Fig. 5; table 12 reports the interaction energy between the inhibitors and the Fe^{2+} iron as well as the bond distances between the Fe^{2+} and the electron donor centers. The optimization of the complex of PNTLD molecule and the Fe^{2+} ion, with the

Fe^{2+} ion in the vicinity of either N atom, results in a geometry in which a single Fe^{2+} ion interact with both N1 and N13 atoms simultaneously.

Table 13. Bond order in the isolated inhibitor molecules and in the complexed inhibitor (B3LYP/6-31G (d,p) results *in vacuo*)

PNTLD			PNTZ			PNXZ			PNZ		
Bond	In isolated	In complex	Bond	In isolated	In complex	Bond	In isolated	In complex	Bond	In isolated	In complex
N1-C2	1.81	1.36	S1-C2	0.97	0.92	O1-C2	0.86	0.72	N1-C2	1.29	1.07
C2-C3	1.07	1.35	C2-C3	1.42	1.42	C2-C3	1.46	1.41	C2-C3	1.24	1.34
C3-C4	1.69	1.44	C3-C4	1.43	1.45	C3-C4	1.40	1.44	C3-C4	1.59	1.47
C4-O4	1.00	1.16	C4-C5	1.44	1.41	C4-C5	1.46	1.36	C4-C5	1.26	1.28
C4-C5	0.97	0.98	C5-C6	1.44	1.43	C5-C6	1.42	1.50	C5-C6	1.59	1.55
C5-C6	0.98	1.81	C6-C7	1.40	1.44	C6-C7	1.41	1.31	C6-C7	1.24	1.23
C6-C7	1.82	1.12	C7-N8	0.95	0.74	C7-N8	0.90	0.96	C7-N8	1.29	1.32
C7-C8	1.12	0.95	N8-C9	0.95	0.75	N8-C9	0.90	0.96	N8-C9	1.29	1.22
C8-C9	0.96	0.99	C9-C10	1.40	1.43	C9-C10	1.41	1.31	C9-C10	1.24	1.25
C9-O9	0.94	0.99	C10-C11	1.44	1.44	C10-C11	1.42	1.50	C10-C11	1.59	1.45
C9-C10	0.96	0.94	C11-C12	1.44	1.41	C11-C12	1.46	1.36	C11-N12	1.26	1.41
C10-C11	0.97	1.04	C12-C13	1.43	1.45	C12-C13	1.40	1.44	C12-C13	1.59	1.31
C11-N12	1.81	1.57	C13-C14	1.42	1.41	C13-C14	1.46	1.41	C13-C14	1.24	1.05
N12-C13	1.06	0.83	C2-C7	1.34	1.29	C14-O1	0.86	0.72	C14-N1	1.29	1.04
C13-C14	0.93	0.93	C9-C14	1.34	1.27	C2-C7	1.33	1.28	C2-C7	1.16	1.12
N1-C14	0.98	0.83	S1-C14	0.97	0.92	C9-C14	1.33	1.28	C9-C14	1.16	1.24
C13-C8	1.64	1.71									
C14-C5	0.96	0.98									

The charges on Fe ion decreases from 2e to 1.234e, which suggests that 0.766e charge has been transferred to the metal ion. Table 13 shows the bond order of the inhibitors in complexation with the metal ion. A comparison of the bond orders in the isolated and in the complexed inhibitors suggests that the bond order of the N1-C1, N1-C14, C11-N12 and N12-C13 bond decreases on complexation, which indicates that there is a decrease in the charge density in these bonds. This decrease in the charge density may be related to the charge transfer from the inhibitor to the metal surface. In this way, charge transfer mechanism is the most probable mode of interaction between the metal and the inhibitor molecule.

The optimization of the PNTZ molecule and the Fe^{2+} ion (with the Fe^{2+} ion in the vicinity of either S1 or N8 atom) results in a geometry in which the Fe^{2+} ion interact with both S1 and N8 simultaneously. This geometry is a consequence of the fact that the lone pair of electrons on each heteroatom is directed on the equatorial side of the heteroatoms. Therefore, because the Fe ion interacts with the lone pair of electrons, it preferentially interacts with the lone pair of both heteroatoms simultaneously. On interaction with PNTZ, the partial atomic charge on Fe atom decreases from 2e to 1.167e, which suggests that the amount of charge transferred to iron is 0.833e, which is higher than the amount of charge transferred to Fe ion when interacting with PNTLD, which may be a consequence of the fact that N8 in PNTZ has more negative charge than either N1 or N12 in PNTLD. However, the interaction energy between iron and the inhibitor is 59.755 kcal/mol higher for the PNTLD-Fe complex than for the PNTZ-Fe complex, which may be a consequence of the better geometry arrangement of the PNTLD-Fe complex; in the PNTLD, the bond distance between Fe and

the N1 and N12 atoms is 1.923Å and 1.989 Å respectively while in PNTZ the bond distance between Fe and either S1 and N8 are longer, being 2.347Å and 2.031Å respectively. A comparison of the bond order in the PNTZ and in the PNXZ-Fe shows that the S1-C2, S1-C14, C7-N8, N8-C9, C2-C7 and C9-C14 bonds have smaller bond order in the complex than in the isolated PNTZ molecule, which indicates that there is a decrease in the charge density in these bonds due to the interaction between the inhibitor and the Fe ion. Such a decrease in the bond order may be related to the charge transfer between the inhibitor molecule and the Fe ion in which the inhibitor donates electrons to the vacant or partially occupied d orbitals of the metal.

Table 14. The electronic configuration and the spin density of iron in the isolated and in the complexes of iron and the studied inhibitors. B3LYP/6-31G (d,p) results *in vacuo*

Structure	Electronic configuration	Spin density
isolated Fe	[core]3d(6.00)	4.000
PNTLD-Fe	[core]4S(0.28)3d(6.16)4p(0.03)	3.788
PNTZ-Fe	[core]4S(0.27)3d(6.24)4p(0.02)	3.819
PNXZ-Fe	[core]4S(1.02)3d(6.00)4p(0.02)	4.934
PNZ-Fe	[core]4S(0.27)3d(6.21)4p(0.03)	3.741

The optimization of the PNXZ molecule and the Fe^{2+} ion, with the Fe^{2+} ion in the vicinity of O1 atom, results in a geometry in which the Fe^{2+} ion interact with only O1. In comparison with the isolated Fe^{2+} ion, the partial atomic charge on Fe atom decreases from 2e to 0.897e, suggesting that the amount of charge transferred to iron is 1.103e. The Mulliken spin density for isolated iron is 4.000 while its spin density in the PNXZ-Fe^{2+} complex is 4.934 which suggests that the added electrons occupy an empty orbital and have the same spin as the other four unpaired electrons in the d orbitals of iron. This is also confirmed by the electronic configuration of iron in the complex (table 14) that shows that nearly all the added electrons are located in 4S orbital. The interaction energy of the PNXZ-Fe^{2+} is 22.183 kcal/mol lower than that of PNTZ-Fe^{2+} complex, suggesting that a simultaneous interaction of iron with two donor centers results in stronger binding than when iron interact with only one donor centre. A comparison of the bond order in the isolated PNXZ and the inhibitor interacting with the metal surface (PNTZ-Fe^{2+}) indicates that O1-C2, C4-C5, C6-C7, C9-C10, C10-C11, C11-C12, C14-O1, C2-C7 and C9-C14 bonds have a significant decrease in the bond order. The decrease in the bond order is related to the decrease in the charge density in these bonds and indicates that the charge transfer from the inhibitor to the metal surface could be the mechanism responsible for the binding of the inhibitor onto the metal surface.

The optimization of the PNZ molecule and the Fe^{2+} ion, with the Fe^{2+} ion in the vicinity of N1 atom, results in a geometry in which the Fe^{2+} ion interact with both the N1 atom and C13 atom. In comparison with the isolated Fe^{2+} ion, the partial atomic charge on Fe atom decreased from 2e to 1.174e, indicating that the amount of charge transferred to iron is 0.826e. The interaction energy of the PNZ-Fe^{2+} is higher than that of PNXZ-Fe^{2+} complex by 6.434 kcal/mol, showing that a simultaneous interaction of iron with two donor centers (N1 and C13) results in stronger binding than when the iron atom interact with only one donor centre (as in PNXZ-Fe^{2+} complex). The bond separation distance

between iron and the donor atoms in PNZ (N1 and C13) are also shorter than the bond separation distance between iron and the donor atom in PNXZ (O1), also indicating that the interaction between iron and PNZ are stronger than between iron and PNXZ. A comparison of the bond order in the isolated PNZ and the inhibitor interacting with the metal surface (PNZ-Fe^{2+}) indicates that N1-C2, C3-C4, C10-C11, C13-C14 and C14-N1 bonds have a significant decrease in the bond order; the C2-C3, C11-C12 and the C9-C14 bond show an increase in the bond order.

The variation (i.e., increase or decrease) in the bond order of some of the bonds in the inhibitor molecules when complexed with Fe (II) ion, indicate charge transfer to the metal surface or internal charge transfer within the inhibitor molecule. To better investigate the type of interactions involving the inhibitor molecule and the Fe ion, the second-order perturbative estimates of donor–acceptor interactions, obtained from NBO analysis, was analyzed for each complex. In the complex PNTLD-Fe, the stabilization of the n^*_{Fe} orbital is due to the N1=C2 bond, C11=N12 bond and N1–C14. The n^*_{Fe} orbital stabilization (kcal/mol) in each case is 4.37, 2.42 and 0.60 respectively. Interestingly, there is also an $n_{Fe} \rightarrow \pi^*_{N1=C2}$ back donation of about 1.94 kcal/mol. In structure PNTZ-Fe, the most significant contributions to the stabilization of the n^*_{Fe} orbital are from the lone pairs on N and S atoms; the $n_N \rightarrow n^*_{Fe}$ stabilization contribution is 31.71 kcal/mol and the $n_S \rightarrow n^*_{Fe}$ stabilization contribution is 38.82 kcal/mol. This result suggests that S has greater contribution to the stabilization of the n^*_{Fe} orbital (i.e., it donates more electrons to the n^*_{Fe} orbital, what is not surprising considering that S has less tendency to hold-on to its lone pairs of electrons than does N atom). In the complex PNXZ, the stabilization to the n^*_{Fe} orbital is due to the lone pair of electrons on the O1 atom; the total contribution to the $n_O \rightarrow n^*_{Fe}$ stabilization is 10.67 kcal/mol. In structure PNZ, the strongest contribution to the stabilization of the n^*_{Fe} orbital is from the N1 atom (12.92 kcal/mol). Both PNTLD and PNZ show strong binding to the Fe ion such that the Fe-inhibitor complex in these cases is considered as one fragment rather than two interacting fragments..

3.5. Quantitative structure activity relationship (QSAR)

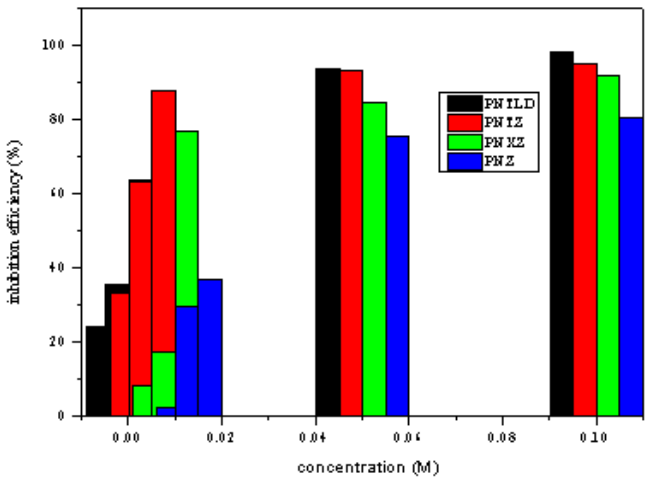

Figure 6. Plot of inhibition efficiency (%IE) versus concentration (M) for phenazine (PNZ), phenothiazine (PNTZ), phenoxazine (PNXZ) and 1, 12-phenathroline (PNTLD) at 303K.

Although the trends in most of the quantum chemical parameters have not entirely correlated with the trend in the experimentally determined inhibition efficiencies of the inhibitors, it is possible that more than one quantum chemical parameters need to be considered simultaneously to correlate with experimentally determined inhibition efficiencies.

Table 15. Equations derived from quantitative structure activity relationships (QSAR) for a combination of quantum descriptors obtained from B3LYP/6-31G (d,p) results

Quantum descriptors	Equation obtained	R^2	SSE	RMSE
	Linear multiple regression equations			
E_{HOMO}, MV	%IE = 7.869*E_{HOMO}+0.584*MV + 17.302	0.998	0.329	**0.574**
E_{HOMO},Pol	%IE = 9.013*E_{HOMO}+7.174*Pol –265.751	0.998	0.418	**0.647**
E_{LUMO}, MV	%IE = 4.460*E_{LUMO}+0.569*MV –16.819	0.994	1.136	**1.066**
E_{HOMO}, μ	%IE = 2.408*E_{HOMO}+4.933*μ + 94.921	0.993	1.266	**1.125**
E_{LUMO}, pol	%IE = 5.089*E_{LUMO}+6.955*Pol –295.936	0.992	1.455	**1.206**
ΔE, μ	%IE = 3.504*ΔE+4.835*μ + 67.395	0.997	0.521	**0.721**
ΔE, MV	%IE = 10.165*ΔE+0.549*MV –60.932	0.984	2.917	**1.708**
ΔE, pol	%IE = 11.544*ΔE+6.666*Pol –334.163	0.980	3.723	**1.930**
ΔE, ΔN	%IE = -229.358*ΔE–2036.671*ΔN + 2033.075	0.992	1.465	**1.211**
μ, MV	%IE = 6.651*μ–0.191*MV + 116.860	0.983	3.153	**1.776**
μ, pol	%IE = 6.429*μ–2.057*Pol + 195.432	0.984	2.891	**1.700**
μ,χ	%IE = 4.905*μ–1.805*χ + 87.929	0.994	1.038	**1.019**
	non-linear multiple regression equations			
ΔE, μ	%IE = (7.563 x 10^{-3}ΔE+7.550 x 10^{-3}μ –1.170) *C_i *100/(1+(7.563 x 10^{-3}ΔE+7.550 x 10^{-3}μ –1.170))	0.998	0.359	**0.599**
E_{HOMO}, μ	%IE = (5.347 x 10^{-3}*E_{HOMO}+7.699 x 10^{-3}*μ –1.110)*C_i *100/(1+(5.347 x 10^{-3}*E_{HOMO}+7.699 x 10^{-3}*μ –1.110))	0.992	1.478	**1.216**
E_{HOMO}, MV	%IE = (1.373 x 10^{-2}*E_{HOMO}+*9.169 x 10^{-4}*MV –1.233) *C_i *100/(1+(1.373 x 10^{-2}*E_{HOMO}+*9.169 x 10^{-4}*MV –1.233))	0.998	0.436	**0.660**
E_{HOMO},Pol	%IE = (1.551 x 10^{-2}*E_{HOMO}+1.127 x 10^{-2}*Pol –1.677)/(1+(1.551 x 10^{-2}*E_{HOMO}+1.127 x 10^{-2}*Pol –1.677))	0.997	0.551	**0.742**
E_{LUMO}, pol	%IE = (8.648 x 10^{-3}*E_{LUMO} + 0.011*Pol –1.729) *C_i *100/(1+(8.648 x 10^{-3}*E_{LUMO} + 0.011*Pol –1.729))	0.989	2.020	**1.421**
ΔE, MV	%IE = (1.714 x 10^{-2}*ΔE+8.547 x 10^{-4}*MV –1.366)/(1+(1.714 x 10^{-2}*ΔE+8.547 x 10^{-4}*MV –1.366))	0.978	4.139	**2.035**
ΔE, pol	%IE = (2.019 x 10^{-2}*ΔE+1.081 x 10^{-2}*Pol –1.821)/(1+(2.019 x 10^{-2}*ΔE+1.081 x 10^{-2}*Pol –1.821))	0.971	5.575	**2.361**
ΔE, ΔN	%IE = (–0.356*ΔE–3.1827*ΔN –1.902)/(1+(–0.356*ΔE–3.1827*ΔN –1.902))	0.993	1.277	**1.130**
μ, pol	%IE = (1.129 x 10^{-2}*μ+–5.284 x 10^{-3}*Pol –0.847)/(1+(1.129 x 10^{-2}*μ+–5.284 x 10^{-3}*Pol –0.847))	0.975	4.604	**2.146**
μ,χ	**%IE = (7.658 x 10^{-3}*μ–3.981 x 10^{-3}*χ –1.125)/(1+(7.658 x 10^{-3}*μ–3.981 x 10^{-3}*χ –1.125))**	**0.994**	**1.105**	**1.051**

R^2 is the coefficient of determination, and *SSE* and RMSE are defined as

The Sum of Squares for Error (SSE) = $\sqrt{\sum_{i=1}^{n}\left(IE_{pred} - IE_{\exp}\right)^2}$

Root Mean Square Error (RMSE) = $\sqrt{\frac{1}{n}\sum_{j=1}^{n}\left(IE_{pred} - IE_{\exp}\right)^2}$

where IE_{pred} is the predicted inhibition efficiency and IE_{exp} is the experimental determined inhibition efficiency, n is the number of observations (compounds) considered.

Fig. 6 shows a plot of the inhibition efficiency versus the concentration for phenazine and related compounds at 303K (PNTLD > PNTZ > PNXZ > PNZ). Similar plot was obtained at 313K (though not shown).

The approach used in correlating more than one quantum chemical parameters to the experimental inhibition efficiency is a statistical approach called quantitative structure activity relationship (QSAR). In this approach mathematical equations are derived which correlates the theoretically estimated inhibition efficiency to the experimentally determined inhibition efficiency. In the current work the Lukovits equations, both linear and non-linear multiple regression equations [29, 30], were found to provide good correlation between the theoretically estimated inhibition efficiency and the experimentally determined inhibition efficiency. The linear multiple regression equation is of the form

$$IE_{theor} = Ax_i\ C_i + B \quad (14)$$

where IE_{theor} is the theoretically estimated inhibition efficiency, A and B are the regression coefficients determined through regression analysis, x_i is a quantum chemical index characteristic of the molecule i, C_i is the experimental concentration of the inhibitor in M.

All the best fit equations are reported in table 15 together with the R^2, SSE and RMSE values. In all the equations, two or more quantum chemical parameters were adequate to form a quantum chemical composite index that was correlated to the experimentally determined inhibition efficiency. The equation with the highest R^2 value, smallest SSE and RMSE values is of the form

$$\%IE = 7.869*E_{HOMO}+0.584*MV + 17.302 \quad (15)$$

This equation suggests that a combination of increasing E_{HOMO} and molecular volume would produce the best correlation between the experimentally determined inhibition efficient and the theoretically estimated inhibition efficiency.

The non-linear multiple regression equation is of the form

$$IE_{theor} = \frac{(AX_i + B)*C_i}{1+(AX_i + B)*C_i}*100 \quad (16)$$

where A and B are constants obtained by regression analysis; X_i is a quantum chemical index characteristic for the molecule; C_i is the inhibitor concentration in M.

All the best fitted equations obtained using the non-linear multiple regression equation are also reported in table 15 together with the R^2, SSE and RMSE values. The high values of R^2 and the small values of SSE and RMSE indicates that there is good correlation between the experimentally determined inhibition efficient and the theoretically estimated inhibition efficiency. Such linear and non-linear approaches gave good and acceptable coefficient of correlation (R^2 = 0.980 – 0.998 for linear and R^2 = 0.975 – 0.998) between the experimentally and calculated inhibition efficiency of the studied compounds as shown in Fig. 7.

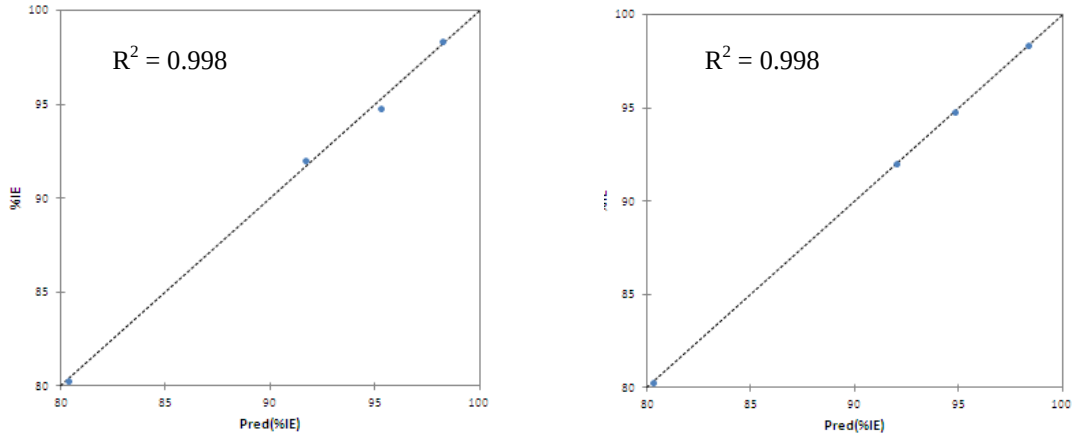

(a) (b)

Figure 7. The plots of experimental inhibition efficiencies versus theoretically estimated inhibition efficiencies (obtained by linear (a) and non-linear (b) equations of Lukovits) for the studied compounds.

3.6. Adsorption isotherm consideration

The experimental data obtained in this study was subjected to further analysis to determine the type of adsorption isotherm it fits into which gives a clue on the mechanism of inhibition. Adsorption isotherms are very important in understanding the mechanism of inhibition of corrosion reaction of metals and alloys. The most frequently used adsorption isotherms are Frumkin, Temkin, Freundlich, Flory-Huggins, Bockris-Swinkel, El-awardy and Langmuir. All these isotherms can be represented as follows:

$$f(\theta, \chi)\exp(-2a\,\theta) = kC \quad (17)$$

where $f(\theta, \chi)$ is the configuration factor which depends on the physical model and the assumptions underlying the derivation of the isotherm. Θ is the degree of the surface coverage, c is the inhibition concentration in the electrolyte, χ is the size ration, a is the molecular interaction parameter and k is the equilibrium constant of the adsorption process. Attempts to fit the experimental data from this study into different isotherms reveal that the data best fitted the Langmuir isotherm. Assumptions of the Langmuir relate the concentration of the adsorbate in the bulk of the electrolyte (c) to the degree of surface coverage (θ) according to the equation below:

$$c / \theta = 1/k_{ads} + c \quad (18)$$

where k_{ads} is the equilibrium constant of adsorption; c is the bulk concentration of the inhibitor. By plotting c/θ versus concentration at the temperature studied, straight lines were obtained (Fig. 8) which proves that Langmuir adsorption isotherm is obeyed for the compounds studied.

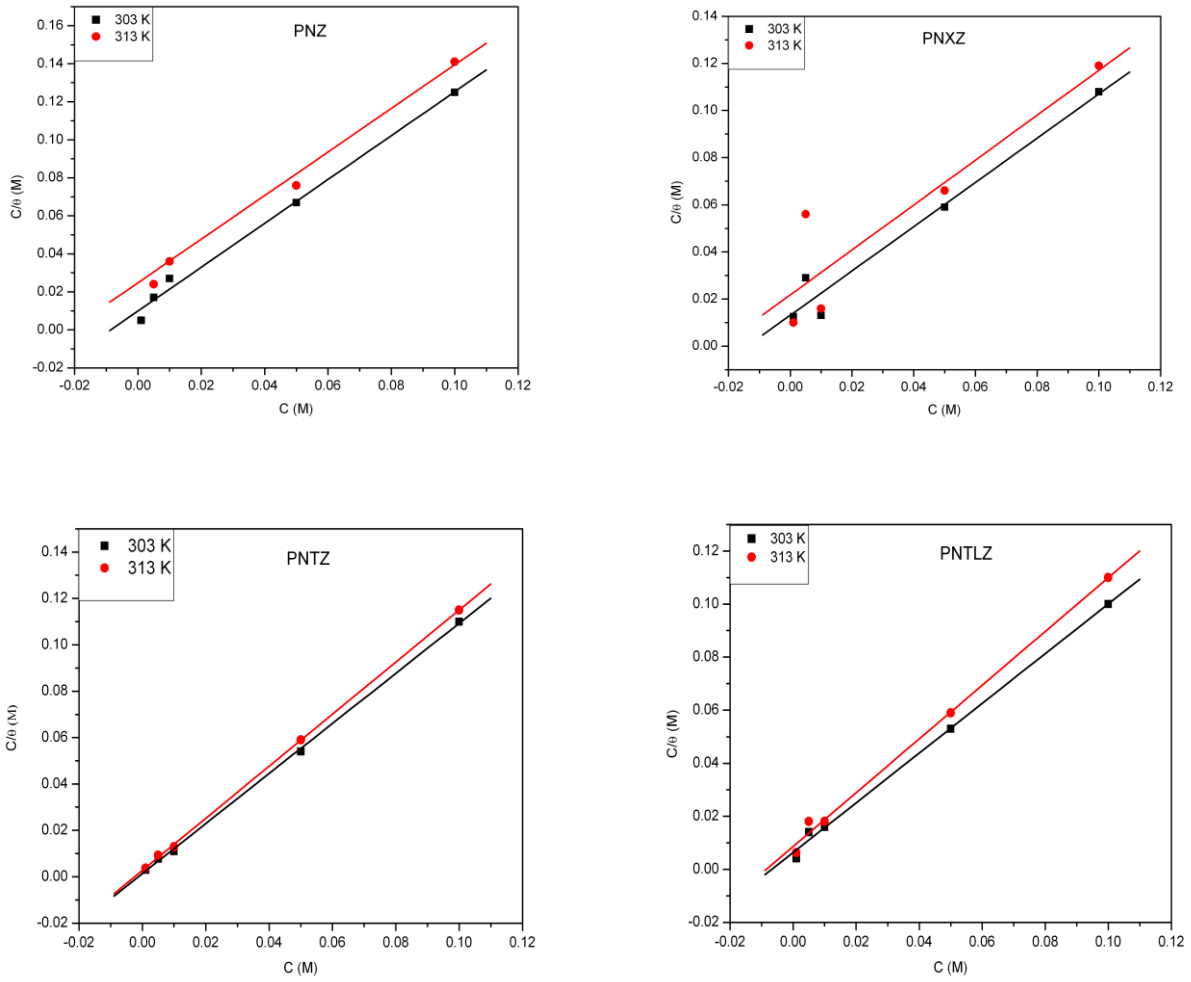

Figure 8. Langmuir adsorption isotherm plot for PNZ, PNXZ, PNTZ and PNTLD at 303 and 313 K

4. CONCLUSIONS

The inhibition efficiency of phenazine (PNZ), phenothiazine (PNTZ), phenoxazine (PNXZ) and 1,12-phenathroline (PNTLD) has been investigate by utilizing experimental techniques and quantum chemical approaches. The quantum chemical results have provided information on the active centers (of the compounds) which would likely interact with the metal surface. Both the analysis of the HOMO and the LUMO and the analysis of the condensed Fukui functions agree on the possible electron donating centers and the possible electron poor centers on the inhibitor molecules. Charges on the atoms have also provided ample information on the electron rich centers of the compounds. Quantitative structure activity relationships study shows that more than one quantum chemical parameters are needed to correlate experimentally determined inhibition efficiencies with theoretically determined inhibition efficiency.

The preference of PNTLD as effectiveness corrosion inhibitor is likely because it has more electron donor centers (that can interact with the metal surface) than other compounds investigated in

this work. Moreover, its interaction with the metal surface results in the strongest interactions because it is capable of interacting with the metal atom by using two electron donor centers simultaneously. The model utilized in this work to describe the interactions between the metal and the inhibitor molecule does not necessarily provide an ideal description of what happens at the metal surface because, in a real situation, there are many Fe^{2+} atoms interacting with the inhibitor molecule and better description may be obtained by using the molecular dynamics method. However, despite the model's weakness, it provides a good qualitative description of the type of mechanism of interaction between the metal and the inhibitor molecules.

The adsorption of the studied compounds onto the metal surface would like be both physical and chemical adsorption; the protonated species would preferentially adsorb chemically onto the metal surface by electrostatically binding to the SO_4 anions that have already adsorbed onto the metal surface. The neutral and the deprotonated species would adsorb chemically into the metal surface by utilizing the electron rich centers. The electron rich centers would donate electrons to the vacant s and d orbitals of the metal thereby effecting a chelation with the metal surface. The experimental data fits the Langmuir adsorption isotherm model.

ACKNOWLEDGEMENT

M.M Kabanda acknowledges the North-West University for a post-doctoral fellowship; E.E Ebenso thanks the National Research Foundation (NRF) of South Africa for funding and L.C. Murulana thanks Sasol-Inzalo Foundation for Postgraduate Bursary.

References

1. S.S. Abdel-Rehim, K.F Khaled, N.A Al-Mobarak, *Arabian. J. Chem*. 4 (2011) 333.
2. P.R. Roberge, Handbook of Corrosion Engineering. McGraw-Hill, New York. (2000)
3. S.A. Umoren, I.B. Obot, E.E. Ebenso, N.O. Obi-Egbedi, *Desalination* 250(2009) 225.
4. E.E. Ebenso, T. Arslan, F. Kandemirli, I. Love, C. Ogretir, M. Saracoglu, S.A. Umoren, *Int. J. Quantum. Chem.* 110 (2010) 2614.
5. R.M. Issa, M.K. Awad, F.M. Atlam, *Appl. Surf. Sci*. 255 (2008) 2433.
6. E. Anouar, P. Košinová, D. Kozlowski, R. Mokrini, J.L. Duroux, P. Trouillas. *Phys. Chem. Chem. Phys.* 11(2009) 7659.
7. P. Perez, R. Contreras, A. Vela, O. Tapia, *Chem. Phys. Lett*. 169 (2007) 419.
8. P. Geerlings, F. De Proft, W. Langenaeker, *Chem. Rev*. 103 (2003) 1793.
9. L. Pauling, The Nature of the Chemical Bond. Cornell University Press, Ithaca, New York (1960).
10. P. Senet, *Chem. Phys. Lett*. 275 (1997) 527.
11. J.B. Foresman, A. Frisch, Exploring Chemistry with Electronic Structure Methods. Gaussian, Inc., Pittsburg, PA (USA), (1995).
12. A.Y Musa, A.A.H. Kadhum, A.B Mohamad, A.A.B. Rahoma, H. Mesmari, *J. Mol. Struct*. 969 (2010) 233.
13. Spartan,10 Wavefunction, Inc. Irvine, CA: Y. Shao, L.F. Molnar, Y. Jung, J. Kussmann, C. Ochsenfeld, S.T. Brown, A.T.B. Gilbert, L.V. Slipehenko, S.V. Levehenko, D.P. O'Neill, R.A. DiStasio Jr., R.C. Lochan, T.Wang, G.J.O. Beran, N.A. Besley, J.M. Herbert, C.Y. Lin, T. Van Voorhis, S.H. Chien, A. Sodt, R.P. Steele, V.A. Rassolov, P.E. Maslen, P.P. Korambath, R.D. Adamson, B. Austin, J. Baker, E.F.C. Byrd, H. Dachsel, R.J. Doerksen, A. Dreuw, B.D. Dunietz, A.D. Dutoi, T.R. Furlani, S.R. Gwaltney, A. Heyden, S. Hirata, C.P. Hsu, G. Kedziora, R.Z.

Khalliulin, P.Klunzinger, A.M. Lee, M.S. Lee, W.Z. Liang, I.Lotan, N. Nair, B.Peters, E.I. Proynov, P.A. Pieniazek, Y.M. Rhee, J. Ritchie, E. Rosta, C.D. Sherrill, A.C. Simmonett, J.E. Subotnik, H.L. Woodcock III, W.Zhang, A.T. Bell, A.K. Chakraborty, D.M. Chipman, F.J. Keil, A. Warshel, W.J. Hehre, H.F. Schaefer, J. Kong, A.I. krylov, P.M.W. Gill and M. Head-Gordon, *Phys. Chem. Chem. Phys.* 8 (2010) 3172.
14. Addinsoft (2012). XLSTAT 2012.1, Data analysis and statistics software for Microsoft Excel, http://www.xlstat.com. Paris, France.
15. N.O. Eddy, *Journal of Advanced Research* 2 (2010) 35.
16. N.O Eddy, F.E Awe, C.E Gimba, N.O Ibisi, E.E Ebenso, *Int. J. Electrochem. Sci*. 6 (2011) 931.
17. N.O. Obi-Egbedi, I.B Obot, M.I El-khaiary, *J. Mol. Struct*. 1002 (2011) 86.
18. L. M. Rodriguez-Valdez, W. Villamisar, M. Casales, J. G. Gonzalez-Rodriguez, A. Martinez-Villafane, L. Martinez L, D. Glossman-Mitnik, *Corros. Sci*. 48 (2006) 4053.
19. P. Fuentealba, P. Perez, R. Contreras, *J. Chem. Phys.* 113 (2000) 2544.
20. L. Cammarata, S. G. Kazarian, P. A. Salterb, T. Welton, *Phys. Chem. Chem. Phys*., 3 (2001) 5192.
21. A.Kokalj, S. Peljhan, M. Finšgar, I. Milošev, *J. Am. Chem. Soc*. 132 (2010) 16657.
22. N. Kovačević, A. Kokalj, *J. Phys. Chem*. C. 115(2011) 24189.
23. H. E. El Ashry, A. El Nemr, S. A. Esawy, S. Ragab, *Electrochim. Acta* 51(2006) 3957.
24. M. Karelson, S. Lobanov, *Chem. Rev.* 96 (1996) 1027.
25. N. O. Eddy, S. A. Odoemelam, *Pigment and Resin Technology* 38 (2009) 111.
26. N. O. Eddy, S. A. Odoemelam, A. O. Odiongenyi, *J. Appl. Electrochem*. 39 (2009) 849.
27. T. Arslan, F. Kandemirli, E. E. Ebenso, I. Love, H. Alemu, *Corros Sci* 51 (2009) 35.
28. E. E. Ebenso, T. Arslan, F. Kandemirli, I. N. Caner, I. Love, *Int. J. Quantum Chem*. 110 (2010) 1003.
29. I.Lukovits, I. Bakó, A. Shaban, E. Kálmán, *Electrochimica Acta* 43 (1998) 131.
30. I.Lukovits, A. Shaban, E. Kalman, *Russian J. Electrochem*. 39 (2003) 177.